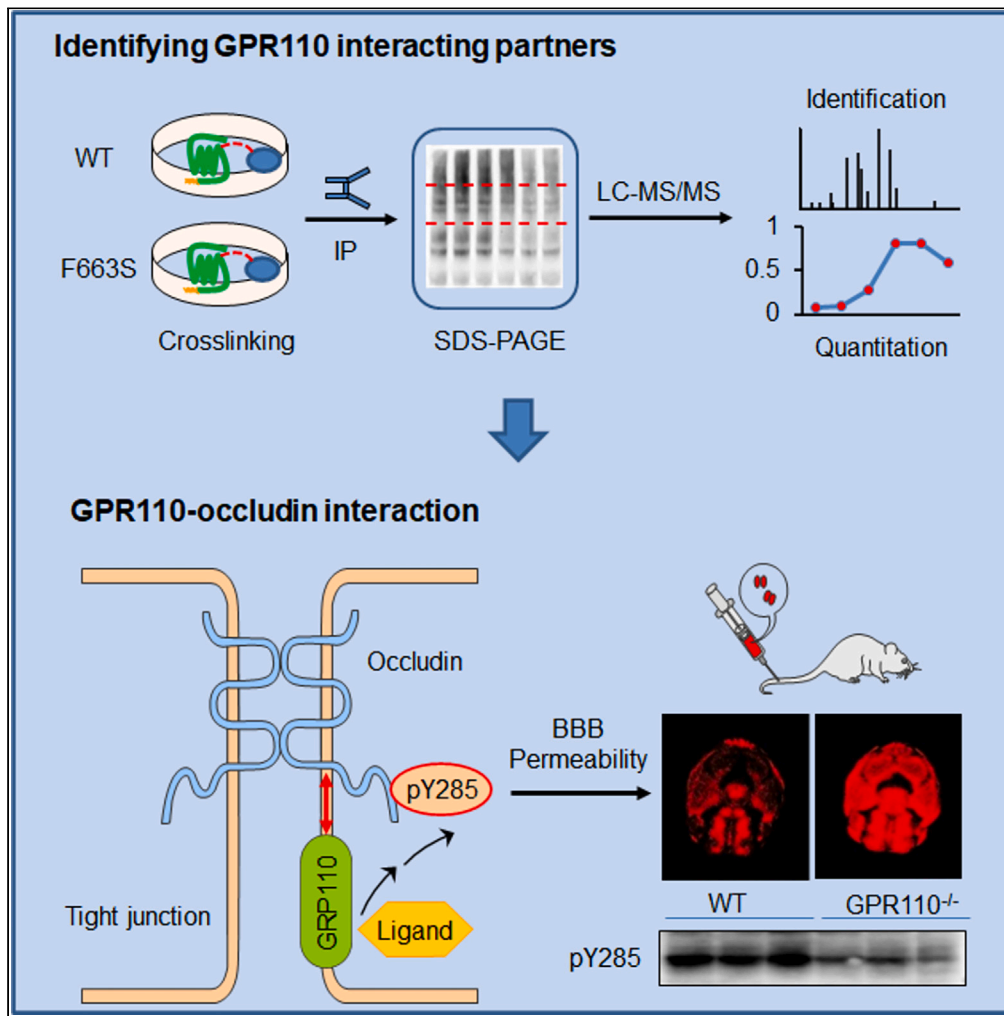**Article**

Interaction between GPR110 (ADGRF1) and tight junction protein occludin implicated in blood-brain barrier permeability

Bill X. Huang, Huazhen Chen, Yuyoung Joo, Heung-Sun Kwon, Cheng Fu, Arthur A. Spector, Hee-Yong Kim

hykim@nih.gov

Highlights

GPR110 interacts with the tight junction protein occludin

GPR110 KO results in a leaky blood-brain barrier (BBB)

Defective BBB function is accompanied by reduced Y285 phosphorylation of occludin

GPR110 activation increases the Y285 phosphorylation of occludin

Article

Interaction between GPR110 (ADGRF1) and tight junction protein occludin implicated in blood-brain barrier permeability

Bill X. Huang,[1] Huazhen Chen,[1] Yuyoung Joo,[1] Heung-Sun Kwon,[1] Cheng Fu,[1] Arthur A. Spector,[1] and Hee-Yong Kim[1,2,*]

SUMMARY

Activation of adhesion receptor GPR110 by the endogenous ligand synaptamide promotes neurogenesis, neurite growth, and synaptogenesis in developing brains through cAMP signal transduction. However, interacting partners of GPR110 and their involvement in cellular function remain unclear. Here, we demonstrate using chemical crosslinking, affinity purification, and quantitative mass spectrometry that GPR110 interacts with the tight junction adhesion protein occludin. By removing non-specific partners by comparing the binding proteins of GPR110 WT and an inactive mutant exhibiting impaired surface expression, occludin was distinguished as a true binding partner which was further confirmed by reciprocal co-immunoprecipitation assay. Deletion of GPR110 in mice led to the disruption of blood-brain barrier (BBB) and reduced occludin phosphorylation at Y285 in the brain. The Y285 phosphorylation increased upon the ligand-induced activation of GPR110. These data suggest an important role of GPR110-occludin interaction in BBB function and association of previously unknown GPR110-dependent occludin phosphorylation at Y285 with BBB integrity.

INTRODUCTION

Adhesion G-protein coupled receptors (aGPCR), comprising 33 members in humans, are the least understood subfamily of GPCRs. These cell surface proteins are characterized by a large ectodomain containing adhesion protein binding domains and a GPCR autoproteolysis inducing (GAIN) domain located immediately before the seven-transmembrane (7TM) domain.[2] Besides signaling through G proteins, these unique receptors are thought to play an important role in cellular adhesion. Growing evidence has demonstrated that aGPCR possess various physiological functions, and several aGPCRs have been linked to human diseases.[3–6] Considerable progress over the last decade has been made in identifying the ligands, understanding the structure and function of the self-cleavable GAIN domain, and explaining the activation and signaling mechanisms of aGPCRs.[7–11] Most recently, cryogenic electron microscopy (cryo-EM) structures for several aGPCRs that support a tethered agonism have been reported.[12–16] However, due to complexity and diversity, more than half of aGPCRs remain orphan, and many functions of aGPCRs and their underlying molecular mechanisms for activation are still unknown.[17] Particularly, few attempts have been made to investigate protein-protein interactions which are required for the proper function and regulation of these receptors. To date, most aGPCRs are without identified interacting partners, further hindering the elucidation of the physiological effects of these receptors.[18]

GPR110 (ADGRF1) belongs to group VI among nine distinct subfamilies of aGPCRs. It is highly expressed in the kidney, neural stem cells, and the brain during development.[8] GPR110 has been deorphanized as the functional receptor for synaptamide (N-docosahexaenoylethanolamine), an endocannabinoid-like metabolite endogenously synthesized from docosahexaenoic acid (DHA, 22:6n-3) which is the major omega-3 fatty acid in the brain. Activation of GPR110 by synaptamide stimulates cAMP signal transduction in a $G_{\alpha s}$-dependent manner, promoting neurogenesis, neurite growth, and synaptogenesis during development.[8] GPR110 knockout abolished the synaptamide-induced bioactivity and GPR110 knockout mice show significant deficits in object recognition and spatial memory.[8] GPR110 signaling also attenuates
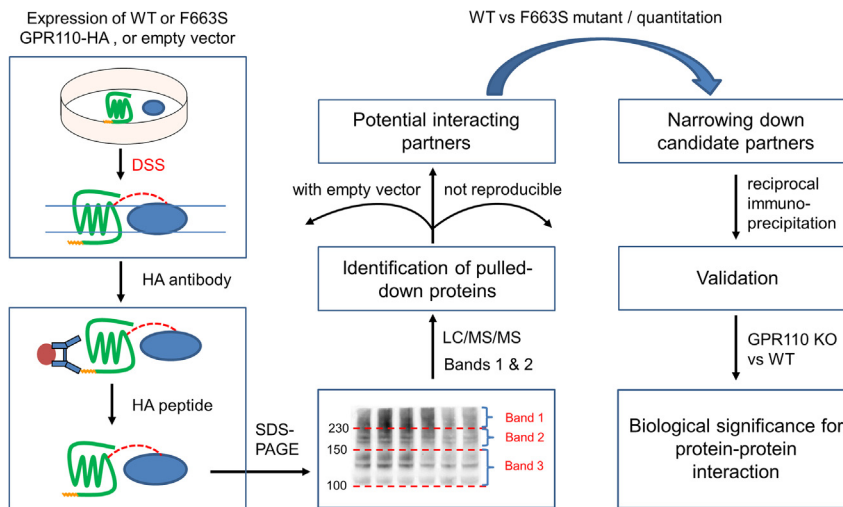
Figure 1. Strategy for the identification of GPR110-interacting partners in living cells
DSS-crosslinking was performed on HEK cells expressing with WT or F663S GPR110-HA or empty vector. GPR110 and interacting partners were pulled down followed by SDS-PAGE and MS analysis. Mutagenesis and quantitative MS were used to narrow down the likely candidates for interacting partners. DSS, disuccinimidyl suberate.

lipopolysaccharide-induced neuroinflammation.[19,20] More recently, we have demonstrated that synaptamide specifically binds to the GAIN domain of GPR110 causing an intracellular conformational change that triggers downstream signaling events.[21] To further explore the function of GPR110, in the present study, we investigated GPR110-interacting proteins in living cells.

Chemical crosslinking combined with affinity purification (AP) and mass spectrometry has emerged as an important tool for probing protein-protein interactions under physiological conditions.[22–25] The strategy involves the affinity purification of the interacting partners that are captured by a crosslinker in living cells followed by SDS-PAGE separation and mass spectrometry-based analysis of the selected gel bands. The approach is sensitive to the identification of interacting proteins that are weakly or transiently bound. A major limitation of this approach is the high false-positive rate, because not only interacting partners but also proteins that indirectly interact with the target protein or are non-specifically bound to the affinity matrix can be detected.[26]

Here, we devised a strategy using mutagenesis and quantitative high-resolution mass spectrometry to distinguish true binding partners from artifacts. We found that the tight junction protein occludin interacts with GPR110 at the cell surface. After validation with reciprocal immunoprecipitation, we evaluated the role of GPR110 in tight junction integrity based on blood-brain barrier (BBB) permeability in GPR110 KO compared to WT mice. Our data suggest a new role of GPR110 in BBB function and implicate a newly recognized GPR110-dependent occludin phosphorylation in the BBB integrity.

RESULTS

Potential GPR110 interacting partners in living cells identified by chemical crosslinking, affinity purification, and mass spectrometry

To capture the GPR110-protein interactions, disuccinimidyl suberate (DSS), an amine-reactive *N*-hydroxysuccinimide ester, was introduced into HEK cells expressing GPR110 tagged with HA at the *C*-terminal. GPR110 and its interacting partners linked by DSS were pulled down by immunoprecipitation with HA antibody. The co-immunoprecipitates were separated by SDS-PAGE, digested with trypsin, and analyzed by LC/MS/MS (Figure 1). To filter out the non-specific proteins, identical experiments were performed in parallel with cells overexpressing HA-tagged empty vector control. Proteins identified from this negative control were considered background proteins. In addition, proteins that were not reproduced in three independent experiments were filtered out.[27,28] With these criteria around 200 proteins were identified as potential GPR110 interacting partners by high-resolution tandem mass spectrometry. For example, Figure 2 shows the unambiguous identification of one of the three unique occludin peptides by tandem mass spectrometry. Both GPR110
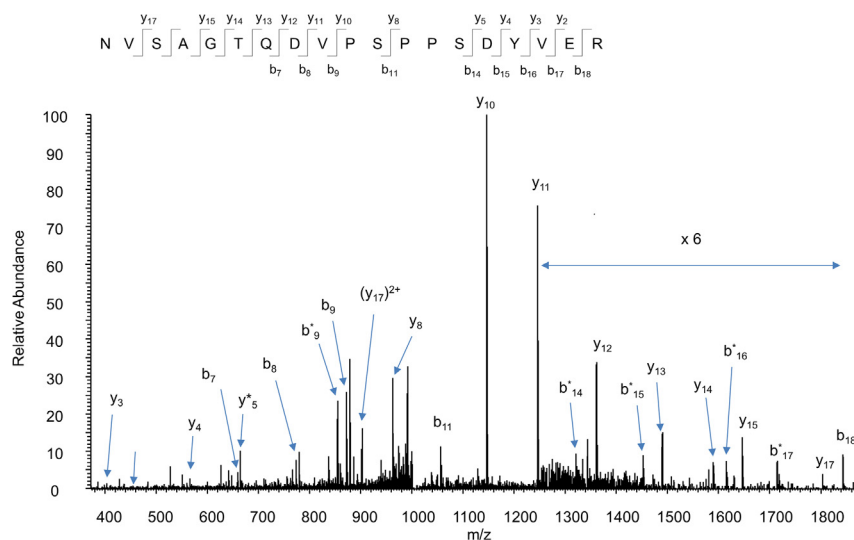
Figure 2. Mass spectrometric identification of occludin co-immunoprecipitated with GPR110

The MS/MS data identifies a unique occludin peptide digested from the GPR110 pull-down proteins after in-cell crosslinking. The amino acids are represented with single-letter abbreviations. N-terminal b (or b*, b-NH$_3$) ions and C-terminal y ions resulting from the amide bond cleavage are labeled.

(~130 kDa) and occludin (~59 kDa) were identified from the gel band that was centered at about 180 kDa (~160-230 kDa) (Figure S1), the molecular weight range of these two proteins after crosslinking.

Narrowing down true binding partners of GPR110 by mutagenesis and quantitative high-resolution mass spectrometry

Arguably less than 10% of proteins identified by a co-IP/mass spectrometric approach are *bona fide* interacting partners even after effectively filtering out a large number of non-specific proteins based on the negative control and reproducibility status. To narrow down the likely candidates for real partners, we took advantage of the cellular location of GPR110. Like other GPCRs, the presence of GPR110 at the plasma membrane is a prerequisite step for its activation. The expression of the WT GPR110 at the cell surface was clearly indicated by non-permeable immunostaining or cell surface biotinylation assay when compared to the expression of the empty vector M45 (Figure 3A). Interestingly, we found that the GPR110 F663S mutant, which was initially identified in a schizophrenic case from the Swedish exome sequencing study, is not properly expressed in the plasma membrane (Figure 3A). Consistent with the impaired cell surface expression, the F663S mutant failed to trigger GPR110 signaling in HEK cells upon ligand stimulation evaluated by CRE-luciferase assay (Figure 3B). Due to its lack of availability at the plasma membrane, this mutant can be used as the negative control for identifying the binding partners of the functional GPR110 receptor with confidence. To identify GPR110-interacting proteins, high-resolution mass spectrometry-based label-free protein quantitation was performed for the GPR110-immunopurified DSS-crosslinked proteins from cells expressing either F663S or WT GPR110 (Figure 3C, inset). Among the 200 potential interacting proteins, 20 proteins, mostly plasma membrane proteins, showed considerably less association with the F663S mutant as compared to WT GPR110. For example, the interaction of the tight junction protein occludin with the F663S mutant was five times less than WT GPR110 (Figure 3C, Supplemental data 1). These 20 proteins are most likely the real binding partners of functional GPR110 in living cells. Proteins that were found to interact similarly with the mutant or WT GPR110, such as transmembrane p24 trafficking protein family member 8 (TMED8, Figure 3C, Supplemental data 1), were considered background proteins, although a physical interaction of these proteins with GPR110 in other organelles cannot be excluded. Considering that both occludin and GPR110 have adhesion properties and occludin plays a critical role in tight junctions at the blood-brain barrier (BBB),[29] we set out to further examine their interaction and biological relevance.

Confirmation of GPR110-occludin interaction

Reciprocal immunoprecipitation assays were used to confirm the interaction of GPR110 with occludin identified by the mass spectrometry-based approach. Lysates from HEK cells expressing GPR110 WT or the
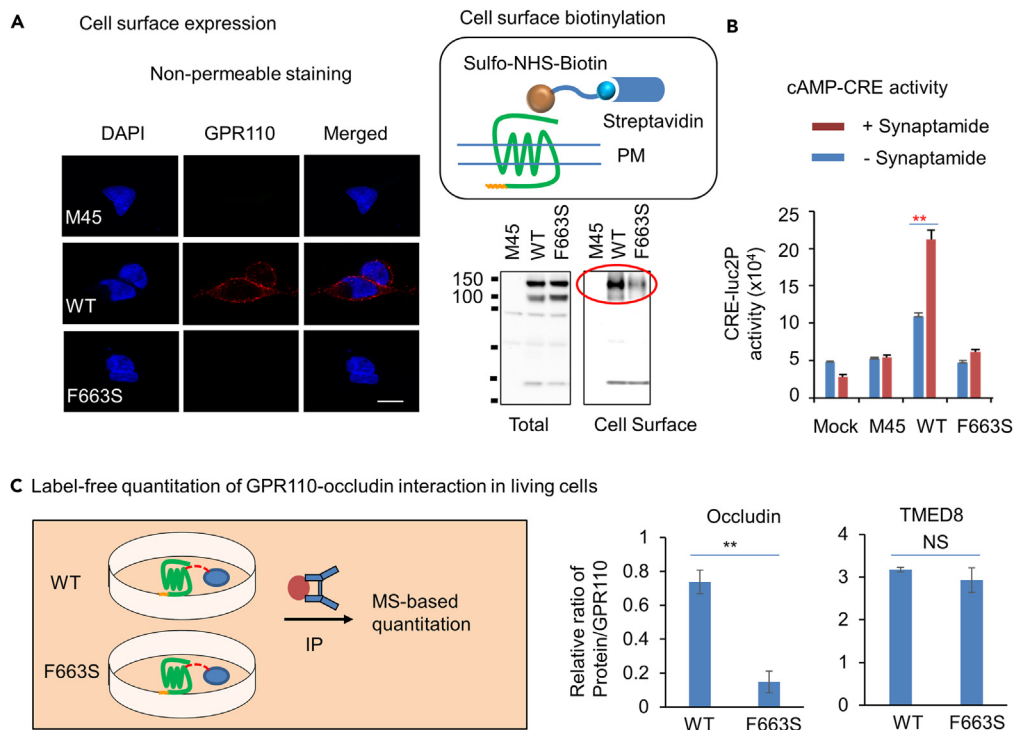
Figure 3. Identification of true GPR110-interacting partners using mutagenesis combined with quantitative mass spectrometry

(A) Impaired expression of GPR110 F663S mutant on the cell surface. HEK cells overexpressing GPR110 WT or F663S were subjected to immunofluorescence staining or cell surface biotinylation. Scale bar, 10 μm.

(B) cAMP production abolished in F663S mutant after GPR110 activation by the extracellular addition of synaptamide. CRE-luciferase assay was used to detect cAMP. M45, empty vector.

(C) Quantitative mass spectrometric analysis of GPR110-occludin interaction. Cells expressing F663S or WT GPR110 were subjected to in-cell crosslinking and immunoprecipitation. The co-immunoprecipitated GPR110 and occludin were analyzed using label-free quantitative mass spectrometry. Significant reduction of occludin observed in cells expressing F663S mutant compared to WT indicated specific interaction of occludin with GPR110 expressed on the cell surface. The interaction of TMED8 with F663S mutant and WT GPR110 was similar, indicating that TMED8 is a non-specific interacting partner. F663S, GPR110 F663S mutant. Statistical analysis was performed using unpaired Student's *t* test (**p < 0.01). Data are means ± SEM of biological replicates (n = 3). NS, not significant.

F663S mutant were subjected to immunoprecipitation with anti-HA and anti-occludin antibodies. When GPR110 was pulled down by the anti-HA antibody, occludin was detected (Figures 4A and S2) and GPR110 was detected with the anti-occludin antibody (Figure 4B). Consistent with the mass spectrometric quantitation, immunoblotting showed significantly less association of occludin with F663S mutant than WT GPR110. The reciprocal immunoprecipitations with quantitative western blot analysis provided independent evidence for the interaction of GPR110 with occludin.

Blood-brain-barrier disruption by GPR110 depletion evaluated with near-infrared whole-brain imaging

Occludin is known to regulate the paracellular barrier of endothelial tight junctions. In addition, it has been reported that the gene depletion of GPR116, an adhesion receptor closely related to GPR110, is associated with BBB disruption.[30] These findings prompted us to examine the biological role of the newly identified GPR110-occludin interaction in the BBB. To evaluate the expression of GPR110 and occludin in the brain endothelium, we isolated intact microvessels from the brain cortex of newborn and adult mice using a non-enzymatic protocol with minimal degradation of RNA (Figures 5A and S3).[31] Compared to the cortical level, the occludin mRNA level was augmented in the microvessels from both adult and newborn brains, as expected from the enrichment of endothelial cells in microvessels (Figures 5A and S3). Although GPR110 expression in the brain is known to diminish in adulthood compared to the newborn stage,[8] GPR110 was

A IP: HA, IB: Occludin
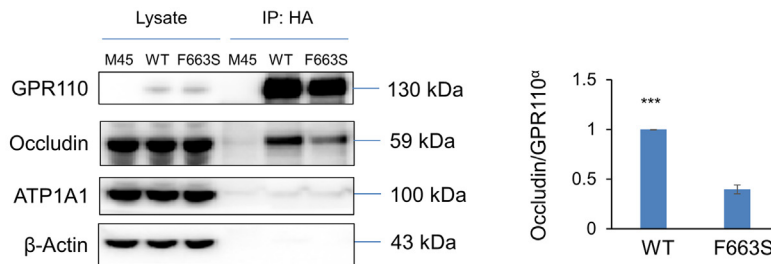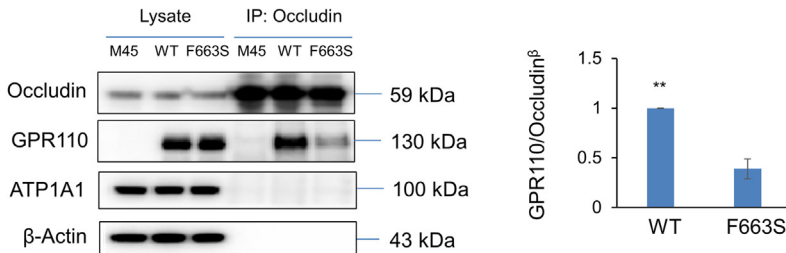

B IP: Occludin, IB: HA

Figure 4. Reciprocal immunoprecipitation assays for the verification of occludin as the true GPR110-interacting partner

Cells expressing F663S or WT GPR110 were subjected to immunoprecipitation with anti-HA antibody (A) or anti-occludin antibody (B). The Co-IP partners were detected and quantified by western blotting. M45, empty vector. ATP1A1 was used as a membrane protein marker. $^{\alpha}$, normalized to occludin in the lysate. $^{\beta}$, normalized to GPR110-HA in the lysate. Statistical analysis was performed using unpaired Student's *t* test (**p < 0.01, ***p < 0.001). Data are means ± SEM of biological replicates (n = 3).

found enriched in the microvessels from adult brains (Figure 5A) as in the case with the newborn brains (Figure S3). We next evaluated the BBB property in the GPR110 knockout adult mouse brains in which GPR110-protein interaction is obviously absent, in comparison to GPR110 WT brains. After the intravenous injection of Rhodamine 800 (R800), a small near-infrared dye for evaluating BBB disruption through paracellular diffusion, the accumulation of R800 in the brain was examined by whole brain imaging.[30,32] As shown in Figure 5B, similar fluorescent images of the brain were observed for the R800-or vehicle-treated WT mice, presumably resulting from the background fluorescence in the tissue. The R800 accumulation in the perfused normal brain was negligible in WT, as reported previously.[32] However, substantial accumulation of R800 was detected in the GPR110-depleted mouse brains (Figure 5B), indicating a considerable disruption of the BBB in the GPR110 KO mice.

Decrease of occludin phosphorylation at Y285 in GPR110 knockout mice

Since occludin function depends on its phosphorylation at various sites in the *C*-terminal domain[33–36] (Figure 6A), we examined whether the GPR110 deficiency alters the occludin phosphorylation status. After whole brain imaging, we homogenized the cerebrum and examined occludin phosphorylation using currently available phospho-occludin antibodies, pY285 (mouse)/pY287 (human), pT382 (mouse) and pS507 (mouse)/pYS508 (human). While no difference was observed for pT382 and pS507 (Figure S4), there was a marked decrease in the phosphorylation of Y285 in the GPR110 KO brains compared to the WT samples (Figure 6B), indicating that GPR110 affects the phosphorylation of occludin at Y285. This GPR110-dependent Y285 phosphorylation of occludin may have a role in regulating BBB permeability. Of note, the occludin level was similar in the mouse brains regardless of the GPR110 status (Figure 6B).

Effect of synaptamide-induced GPR110 activation on occludin phosphorylation and occludin interaction with GPR110

Since the phosphorylation status of occludin at Y285 in the mouse brain was observed to be GPR110-dependent, we examined whether this phosphorylation is influenced by the ligand-induced GPR110
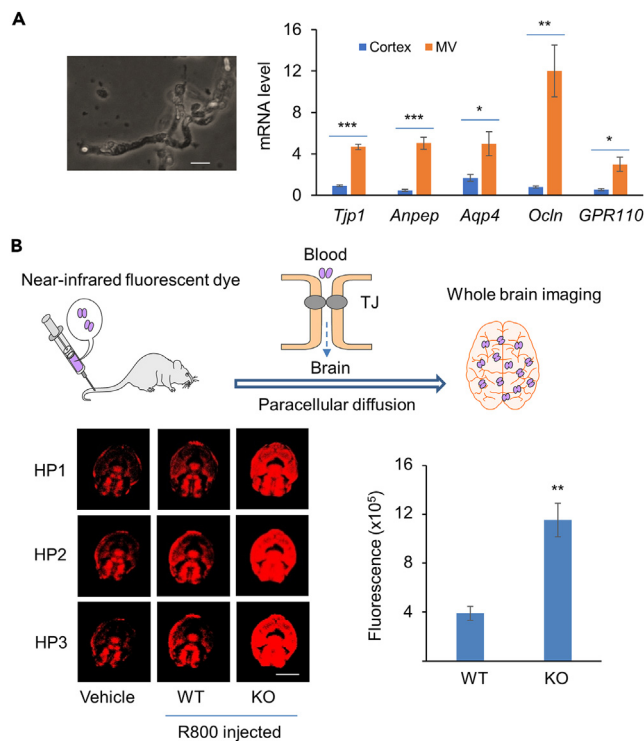
Figure 5. Effect of GPR110 depletion on blood-brain barrier function

(A) Enrichment of GPR110 and occludin in adult mouse brain microvessels. The phase-contrast image shows the microvessels (scale bar, 10 μm) isolated from the cortex. Components of the brain microvessels were assessed by RT-qPCR quantitation. *Tjp1, Anpep,* and *Aqp4* are markers for endothelial cells, pericytes and astrocytes, respectively. GPR110 mRNA level was evaluated with a TaqMan gene expression assay and normalized to the HPRT gene. Other gene levels were evaluated by SYBR™ Green assay and normalized to GAPDH. *Ocln,* occludin.

(B) Representative near-infrared images of mouse brains perfused with Rhodamine 800 dye (R800, ~500 Da) and associated quantitation of R800 accumulation in the mouse brains, showing a significant increase in dye accumulation in GPR110 KO brains. The near-infrared fluorescent dye was injected intravenously into the tail vein in adult WT or GPR110 KO mice (6-month old). The images were taken at several horizontal planes (HP). Scale bar, 0.5 cm. Statistical analysis was performed using unpaired Student's t test (*$p < 0.05$, **$p < 0.01$, ***$p < 0.001$). Data are means $\pm$ SEM of biological replicates (A, n = 4; B, n = 6 for GPR110 KO and n = 4 for WT).

activation. To this end, HEK cells were transfected with GPR110 and stimulated with synaptamide.[8] Interestingly, the phosphorylation of Y287 (corresponding to Y285 in mouse occludin) increased in a time-dependent manner upon treatment with synaptamide (Figure 6C). When HEK cells were transfected with the F663S mutant, however, the ligand-induced increase in phosphorylation was no longer observed (Figure 6C), consistent with the lack of bioactivity observed for this mutant (Figure 3B). We also examined whether the synaptamide-induced GPR110 activation affects GPR110-occludin interaction. HEK cells expressing GPR110 were treated with 10 nM synaptamide for up to 25 min followed by DSS-crosslinking, immunoprecipitation, and mass spectrometry-based analysis. The interaction of GPR110 with occludin remained unaltered although GPR110 activation was evident by the increase of the phosphorylation of CREB upon treatment with synaptamide (Figure 6C). The data indicate that GPR110 interaction with occludin is independent of ligand-induced GPR110 activation, unlike the occludin phosphorylation at Y287.

DISCUSSION

A key to understanding the function and regulation of the less-known adhesion GPCRs is to identify their interacting partners under physiological conditions. In this article, we report a combinational approach to effectively identify the interacting partners of the adhesion GPCR GPR110 in living cells (Figure 1). From nearly 200 potential interacting proteins identified by in-cell chemical crosslinking, immunoprecipitation, and mass spectrometry, we filtered out irrelevant binding partners of GPR110 using F663S, a GPR110 mutant that is minimally expressed on the cell surface (Figure 3A). Revealed by quantitative MS analysis,
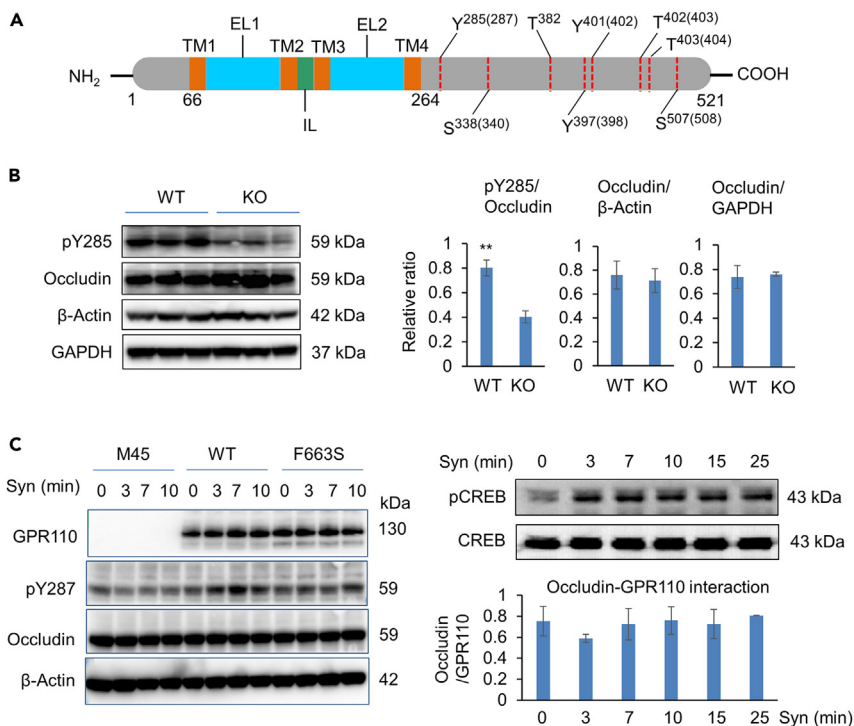
Figure 6. Effect of GPR110 on occludin phosphorylation at Y285

(A) Phosphorylation sites at the C-terminal of mouse occludin (AA 264-521). Corresponding residues in human occludin are indicated in parentheses. TM, transmembrane; EL, extracellular loop, IL, intracellular loop.

(B) Reduced occludin phosphorylation at Y285 in GPR110 KO mouse brains (n = 3).

(C) Effect of synaptamide-induced GPR110 activation on occludin phosphorylation at Y287 and GPR110-occludin interaction in HEK cells. Statistical analysis was performed using unpaired Student's t test (**p < 0.01). Data are means ± SEM of biological replicates (n = 3).

both WT and F663S GPR110 showed similar interaction for most of the 200 potential partners, indicating that these proteins are non-specific binders or their interaction with GPR110 occurs in the organelles other than the plasma membrane. With this approach, we were able to narrow down the GPR110 interacting partners to 20 proteins for further investigation. Selected interactions were confirmed by reciprocal immunoprecipitation assay, the gold standard for the validation of protein-protein interactions. Of note, not only the interaction with WT GPR110, but also the reduced interaction with the F663S mutant, were considered the validation criteria in the reciprocal immunoprecipitation assays (Figure 4). The approach allowed us to effectively identify GPR110 interacting partners for the much-needed functional insight into this receptor.

The interaction of GPR110 with the tight junction protein occludin as well as its enrichment in brain microvessels (Figure 5A) suggests a new role of GPR110 in the BBB. The BBB is composed of brain microvascular endothelial cells, which are connected via tight junction (TJ) proteins including tetraspan membrane proteins claudin and occludin, and junction adhesion molecules. Like claudin, the two extracellular loops of occludin from adjacent endothelial cells are fused tightly together, contributing to the formation of the tight junction, the barrier that regulates the transit of substances through the paracellular pathway (Figure 7). It is believed that while claudin is a key structural component of the BBB, occludin plays a role in regulating TJ assembly and the BBB permeability.[35] Approximately two dozen of GPCRs from all five classes have been shown to influence the structure and function of the BBB.[37,38] It has been reported that in many cases activation/deactivation or gene manipulation of these GPCRs induces changes in the expression of TJ proteins or signaling pathways regulating BBB cytoskeleton organization.[38] For instance, gene silencing of sphingosine 1-phosphate receptor-5, a member of the class A GPCR subfamily, resulted in reduced expression of claudin, occludin, and VE-cadherin, along with decreased BBB function demonstrated by the fluorescent probe FITC-dextran.[39] Adhesion GPCRs uniquely contain various adhesion domains in their long extracellular region and thus are expected to influence cell-cell adhesion as well
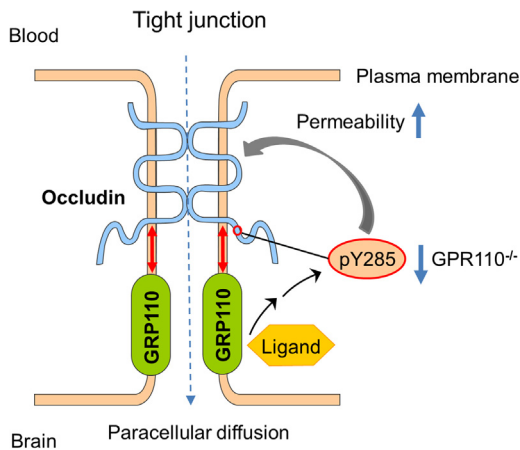
Figure 7. Role of GPR110 in the BBB integrity
GPR110 interacts with tight junction protein occludin and influences paracellular permeability of the blood-brain-barrier (BBB). GPR110 modulates phosphorylation of its interacting partner occludin at Y285 that may also affect BBB integrity as a decrease of pY285 (depicted by a blue downward arrow) is associated with an increase of paracellular permeability (depicted by a blue upward arrow) in GPR110 KO mice.

as tight junctions in the BBB. However, only two aGPCRs, ADGRF5 (GPR116) and ADGRA2 (GPR124), have been found to play a role in the BBB function. GPR116 gene-depletion leads to BBB disruption in mouse brains.[30] Conditional KO of GPR124 is also linked to a leaky BBB.[40] Of note, the exact mechanisms underlying the effect of GPCRs including adhesion GPR116 and GPR124 on the BBB remain unclear. We found that GPR110-depletion led to BBB leakage in adult moue brain, as determined by near-infrared imaging of R800, a small near-infrared fluorescent dye that enters the brain only by paracellular diffusion (Figure 5B). The data clearly indicates that GPR110, an aGPCR with structure closely related to GPR116, also plays a significant role in BBB function. Of note, the leaky BBB may have contributed to impaired cognitive function, a brain phenotype that we discovered previously in GPR110 KO mice.[8] As GPR110 did not affect the occludin expression (Figure 6B), the leaky BBB observed in GPR110 KO was obviously not due to altered expression of occludin. Instead, the GPR110 interaction with occludin may be an important factor for the proper tight junction assembly for BBB integrity (Figure 7).

The discovery of reduced occludin phosphorylation at Y285 in GPR110 KO mice suggests a new mechanism for BBB paracellular diffusion (Figure 7). Occludin contains a large cytoplasmic C-terminal region (aa 266-522) rich in serine, threonine, and tyrosine residues (Figure 6A). The second half of the C-terminal is bound to cytoplasmic scaffolding proteins zonula occludens (e.g. ZO-1), which interacts with actin filaments in the cytoskeleton. These abundant phosphorylation sites have been shown to influence TJ function and BBB permeability.[41] For examples, phosphorylation of T403/T404, T424/T438, and S340 by novel protein kinase Cη, atypical PKCζ, and conventional PKC has been shown to regulate epithelial TJ assembly and/or maintenance.[41,42] Phosphorylation of T382 and S507 by Rho kinase was also shown to reduce BBB tightness in mouse brains.[43] Furthermore, phosphorylation at Y398 and Y402 by c-Src, has been shown to cause the dissociation of zonula occludens-1 (ZO-1) from occludin, which in turn decreases the TJ integrity and increases BBB permeability.[44] The observation that Y285 phosphorylation was significantly reduced in GPR110 KO brains (Figure 6) where increased BBB permeability was detected (Figure 5) suggests that unlike phosphorylation of Y398 and Y402, phosphorylation of Y285 is associated with enhanced BBB integrity. Interestingly, this phosphorylation was elevated by the ligand-induced activation of GPR110 (Figure 6C). While the interaction of GPR110 with occludin was not altered by the ligand stimulation (Figure 6C), it is possible that GPR110 activation produced conformational changes in the GPR110-interacting protein occludin, resulting in the Y285 (or Y287 in human) phosphorylation favored by an upstream kinase. The ligand-induced GPR110 activation, that stimulates the cAMP production and PKA/CREB signaling through $G_{\alpha s}$ coupling,[8] may also enhance the activity of the unknown upstream protein kinases of Y285. Alternatively, GRK recruited after GPR110 activation by synaptamide may play a role in Y285 phosphorylation. Recently, GPR110 has been shown to be able to couple with G_q, G_i, and $G_{12/13}$ in addition to G_s,[16] opening possibilities that Y285 is phosphorylated by upstream kinases activated through any of these G protein signaling pathways. To our knowledge, this is the first report to suggest possible involvement of phosphorylation at Y285/Y287 in occludin function.

In conclusion, we demonstrated for the first time that the aGPCR GPR110 interacts with the tight junction protein occludin and may influence BBB integrity. We also demonstrated the GPR110-dependent

upregulation of the phosphorylation of occludin at Y285/Y287. Occludin phosphorylation at Y285/Y287, a previously unknown function, was found to be negatively associated with BBB permeability. Our data indicate a new role of GPR110 in BBB function, suggesting that GPR110-occludin interaction can be targeted for improving neuropathological conditions including neuroinflammation caused by defective BBB function.

Limitations of the study

While these findings suggest a process by which GPR110 affects BBB integrity, further studies are needed to determine the mechanism by which GPR110 interacts with the TJ protein occludin and promotes the phosphorylation of occludin at Y285. Identification and characterization of the kinase responsible for the phosphorylation of Y285 upon GPR110 activation would be the key to pinpointing the mechanisms more precisely. Determination of the effect of Y285 phosphorylation on the TJ complex assembly and how GPR110 activation affects the interaction of occludin with other TJ proteins such as ZO-1 also would provide additional mechanistic insight.

STAR★METHODS

Detailed methods are provided in the online version of this paper and include the following:

- KEY RESOURCES TABLE
- RESOURCE AVAILABILITY
  - Lead contact
  - Materials availability
  - Data and code availability
- EXPERIMENTAL MODEL AND SUBJECT DETAILS
  - Mice
  - Cell culture
- METHOD DETAILS
  - Plasmid constructs
  - Transfection of HEK293 cells
  - Chemical crosslinking in living cells
  - Synaptamide stimulation
  - Purification of GPR110
  - SDS-PAGE, in-gel digestion and desalting
  - Nano-HPLC MS/MS analysis
  - Identification of proteins
  - Label-free protein quantitation
  - Western blot analysis
  - Luciferase assay for cAMP activity
  - Immunocytochemistry
  - Cell surface biotinylation
  - Isolation and evaluation of cerebral microvessels
  - Real time quantitative PCR (RT-qPCR)
  - Evaluation of the BBB permeability using near infrared fluorescence imaging
- QUANTIFICATION AND STATISTICAL ANALYSIS

SUPPLEMENTAL INFORMATION

Supplemental information can be found online at https://doi.org/10.1016/j.isci.2023.106550.

AUTHOR CONTRIBUTIONS

H-Y.K. directed the research, B.X.H. and H-Y. K. designed the experiments, analyzed data, and wrote the article. B.X.H. performed in cell crosslinking, immunoprecipitation, mass spectrometry-based analysis, microvessel isolation, and whole brain imaging. H.C. performed intravenous injection, perfusion, and

dissection. Y.J. performed dissection and RT-qPCR. H-S. K. performed immunohistochemistry and cAMP assay. C.F. performed cell surface biotinylation assay. A.A.S. provided input and edited the article. All authors reviewed the article and provided input.

DECLARATION OF INTERESTS

The authors declare no competing interests.

REFERENCES

1. Perez-Riverol, Y., Bai, J., Bandla, C., García-Seisdedos, D., Hewapathirana, S., Kamatchinathan, S., Kundu, D.J., Prakash, A., Frericks-Zipper, A., Eisenacher, M., et al. (2022). The PRIDE database resources in 2022: a hub for mass spectrometry-based proteomics evidences. Nucleic Acids Res. *50*, D543–D552. https://doi.org/10.1093/nar/gkab1038.

2. Hamann, J., Aust, G., Araç, D., Engel, F.B., Formstone, C., Fredriksson, R., Hall, R.A., Harty, B.L., Kirchhoff, C., Knapp, B., et al. (2015). International union of basic and clinical pharmacology. XCIV. Adhesion G protein-coupled receptors. Pharmacol. Rev. *67*, 338–367. https://doi.org/10.1124/pr.114.009647.

3. Monk, K.R., Naylor, S.G., Glenn, T.D., Mercurio, S., Perlin, J.R., Dominguez, C., Moens, C.B., and Talbot, W.S. (2009). A G protein-coupled receptor is essential for schwann cells to initiate myelination. Science *325*, 1402–1405. https://doi.org/10.1126/science.1173474.

4. Piao, X., Hill, R.S., Bodell, A., Chang, B.S., Basel-Vanagaite, L., Straussberg, R., Dobyns, W.B., Qasrawi, B., Winter, R.M., Innes, A.M., et al. (2004). G protein-coupled receptor-dependent development of human frontal cortex. Science *303*, 2033–2036. https://doi.org/10.1126/science.1092780.

5. Weston, M.D., Luijendijk, M.W.J., Humphrey, K.D., Möller, C., and Kimberling, W.J. (2004). Mutations in the VLGR1 gene implicate G-protein signaling in the pathogenesis of Usher syndrome type II. Am. J. Hum. Genet. *74*, 357–366. https://doi.org/10.1086/381685.

6. Langenhan, T., Piao, X., and Monk, K.R. (2016). Adhesion G protein-coupled receptors in nervous system development and disease. Nat. Rev. Neurosci. *17*, 550–561. https://doi.org/10.1038/nrn.2016.86.

7. Araç, D., Boucard, A.A., Bolliger, M.F., Nguyen, J., Soltis, S.M., Südhof, T.C., and Brunger, A.T. (2012). A novel evolutionarily conserved domain of cell-adhesion GPCRs mediates autoproteolysis. EMBO J. *31*, 1364–1378. https://doi.org/10.1038/emboj.2012.26.

8. Lee, J.W., Huang, B.X., Kwon, H., Rashid, M.A., Kharebava, G., Desai, A., Patnaik, S., Marugan, J., and Kim, H.Y. (2016). Orphan GPR110 (ADGRF1) targeted by N-docosahexaenoylethanolamine in development of neurons and cognitive function. Nat. Commun. *7*, 13123. https://doi.org/10.1038/ncomms13123.

9. Liebscher, I., Cevheroğlu, O., Hsiao, C.C., Maia, A.F., Schihada, H., Scholz, N., Soave, M., Spiess, K., Trajković, K., Kosloff, M., and Prömel, S. (2021). A guide to adhesion GPCR research. FEBS J. *289*, 7610–7630. https://doi.org/10.1111/febs.16258.

10. Purcell, R.H., and Hall, R.A. (2018). Adhesion G protein-coupled receptors as drug targets. Annu. Rev. Pharmacol. Toxicol. *58*, 429–449. https://doi.org/10.1146/annurev-pharmtox-010617-052933.

11. Vizurraga, A., Adhikari, R., Yeung, J., Yu, M., and Tall, G.G. (2020). Mechanisms of adhesion G protein-coupled receptor activation. J. Biol. Chem. *295*, 14065–14083. https://doi.org/10.1074/jbc.REV120.007423.

12. Barros-Álvarez, X., Nwokonko, R.M., Vizurraga, A., Matzov, D., He, F., Papasergi-Scott, M.M., Robertson, M.J., Panova, O., Yardeni, E.H., Seven, A.B., et al. (2022). The tethered peptide activation mechanism of adhesion GPCRs. Nature *604*, 757–762. https://doi.org/10.1038/s41586-022-04575-7.

13. Ping, Y.Q., Xiao, P., Yang, F., Zhao, R.J., Guo, S.C., Yan, X., Wu, X., Zhang, C., Lu, Y., Zhao, F., et al. (2022). Structural basis for the tethered peptide activation of adhesion GPCRs. Nature *604*, 763–770. https://doi.org/10.1038/s41586-022-04619-y.

14. Qu, X., Qiu, N., Wang, M., Zhang, B., Du, J., Zhong, Z., Xu, W., Chu, X., Ma, L., Yi, C., et al. (2022). Structural basis of tethered agonism of the adhesion GPCRs ADGRD1 and ADGRF1. Nature *604*, 779–785. https://doi.org/10.1038/s41586-022-04580-w.

15. Xiao, P., Guo, S., Wen, X., He, Q.T., Lin, H., Huang, S.M., Gou, L., Zhang, C., Yang, Z., Zhong, Y.N., et al. (2022). Tethered peptide activation mechanism of the adhesion GPCRs ADGRG2 and ADGRG4. Nature *604*, 771–778. https://doi.org/10.1038/s41586-022-04590-8.

16. Zhu, X., Qian, Y., Li, X., Xu, Z., Xia, R., Wang, N., Liang, J., Yin, H., Zhang, A., Guo, C., et al. (2022). Structural basis of adhesion GPCR GPR110 activation by stalk peptide and G-proteins coupling. Nat. Commun. *13*, 5513. https://doi.org/10.1038/s41467-022-33173-4.

17. Rosa, M., Noel, T., Harris, M., and Ladds, G. (2021). Emerging roles of adhesion G protein-coupled receptors. Biochem. Soc. Trans. *49*, 1695–1709. https://doi.org/10.1042/Bst20201144.

18. Knapp, B., and Wolfrum, U. (2016). Adhesion GPCR-related protein networks. Handb. Exp. Pharmacol. *234*, 147–178. https://doi.org/10.1007/978-3-319-41523-9_8.

19. Park, T., Chen, H., Kevala, K., Lee, J.W., and Kim, H.Y. (2016). N-Docosahexaenoylethanolamine ameliorates LPS-induced neuroinflammation via cAMP/PKA-dependent signaling. J. Neuroinflammation *13*, 284. https://doi.org/10.1186/s12974-016-0751-z.

20. Park, T., Chen, H., and Kim, H.Y. (2019). GPR110 (ADGRF1) mediates anti-inflammatory effects of N-docosahexaenoylethanolamine. J. Neuroinflammation *16*, 225. https://doi.org/10.1186/s12974-019-1621-2.

21. Huang, B.X., Hu, X., Kwon, H.S., Fu, C., Lee, J.W., Southall, N., Marugan, J., and Kim, H.Y. (2020). Synaptamide activates the adhesion GPCR GPR110 (ADGRF1) through GAIN domain binding. Commun. Biol. *3*, 109. https://doi.org/10.1038/s42003-020-0831-6.

22. Gingras, A.C., Gstaiger, M., Raught, B., and Aebersold, R. (2007). Analysis of protein complexes using mass spectrometry. Nat. Rev. Mol. Cell Biol. *8*, 645–654. https://doi.org/10.1038/nrm2208.

23. Sinz, A. (2010). Investigation of protein-protein interactions in living cells by chemical crosslinking and mass spectrometry. Anal. Bioanal. Chem. *397*, 3433–3440. https://doi.org/10.1007/s00216-009-3405-5.

24. Yu, C., and Huang, L. (2018). Cross-Linking mass spectrometry: an emerging technology for interactomics and structural biology. Anal. Chem. *90*, 144–165. https://doi.org/10.1021/acs.analchem.7b04431.

25. Richards, A.L., Eckhardt, M., and Krogan, N.J. (2021). Mass spectrometry-based protein-protein interaction networks for the study of human diseases. Mol. Syst. Biol. *17*, e8792. https://doi.org/10.15252/msb.20188792.

26. Bruce, J.E. (2012). In vivo protein complex topologies: sights through a cross-linking lens. Proteomics 12, 1565–1575. https://doi.org/10.1002/pmic.201100516.

27. Amoresano, A., Di Costanzo, A., Leo, G., Di Cunto, F., La Mantia, G., Guerrini, L., and Calabrò, V. (2010). Identification of DeltaNp63alpha protein interactions by mass spectrometry. J. Proteome Res. 9, 2042–2048. https://doi.org/10.1021/pr9011156.

28. Huang, B.X., and Kim, H.Y. (2013). Effective identification of Akt interacting proteins by two-step chemical crosslinking, Co-immunoprecipitation and mass spectrometry. PLoS One 8, e61430. https://doi.org/10.1371/journal.pone.0061430.

29. Yuan, S., Liu, K.J., and Qi, Z. (2020). Occludin regulation of blood-brain barrier and potential therapeutic target in ischemic stroke. Brain Circ. 6, 152–162. https://doi.org/10.4103/bc.bc_29_20.

30. Niaudet, C., Hofmann, J.J., Mäe, M.A., Jung, B., Gaengel, K., Vanlandewijck, M., Ekvärn, E., Salvado, M.D., Mehlem, A., Al Sayegh, S., et al. (2015). Gpr116 receptor regulates distinctive functions in pneumocytes and vascular endothelium. PLoS One 10, e0137949. https://doi.org/10.1371/journal.pone.0137949.

31. Lee, Y.K., Uchida, H., Smith, H., Ito, A., and Sanchez, T. (2019). The isolation and molecular characterization of cerebral microvessels. Nat. Protoc. 14, 3059–3081. https://doi.org/10.1038/s41596-019-0212-0.

32. On, N.H., Savant, S., Toews, M., and Miller, D.W. (2013). Rapid and reversible enhancement of blood-brain barrier permeability using lysophosphatidic acid. J. Cereb. Blood Flow Metab. 33, 1944–1954. https://doi.org/10.1038/jcbfm.2013.154.

33. Cummins, P.M. (2012). Occludin: one protein, many forms. Mol. Cell Biol. 32, 242–250. https://doi.org/10.1128/Mcb.06029-11.

34. Dörfel, M.J., and Huber, O. (2012). A phosphorylation hotspot within the occludin C-terminal domain. Ann. N. Y. Acad. Sci. 1257, 38–44. https://doi.org/10.1111/j.1749-6632.2012.06536.x.

35. Feldman, G.J., Mullin, J.M., and Ryan, M.P. (2005). Occludin: structure, function and regulation. Adv. Drug Deliv. Rev. 57, 883–917. https://doi.org/10.1016/j.addr.2005.01.009.

36. Manda, B., Mir, H., Gangwar, R., Meena, A.S., Amin, S., Shukla, P.K., Dalal, K., Suzuki, T., and Rao, R. (2018). Phosphorylation hotspot in the C-terminal domain of occludin regulates the dynamics of epithelial junctional complexes. J. Cell Sci. 131, jcs206789. https://doi.org/10.1242/jcs.206789.

37. González-Mariscal, L., Raya-Sandino, A., González-González, L., and Hernández-Guzmán, C. (2018). Relationship between G proteins coupled receptors and tight junctions. Tissue Barriers 6, e1414015. https://doi.org/10.1080/21688370.2017.1414015.

38. Pluimer, B.R., Colt, M., and Zhao, Z. (2020). G protein-coupled receptors in the mammalian blood-brain barrier. Front. Cell. Neurosci. 14, 139. https://doi.org/10.3389/fncel.2020.00139.

39. van Doorn, R., Lopes Pinheiro, M.A., Kooij, G., Lakeman, K., van het Hof, B., van der Pol, S.M.A., Geerts, D., van Horssen, J., van der Valk, P., van der Kam, E., et al. (2012). Sphingosine 1-phosphate receptor 5 mediates the immune quiescence of the human brain endothelial barrier. J. Neuroinflammation 9, 133. https://doi.org/10.1186/1742-2094-9-133.

40. Chang, J., Mancuso, M.R., Maier, C., Liang, X., Yuki, K., Yang, L., Kwong, J.W., Wang, J., Rao, V., Vallon, M., et al. (2017). Gpr124 is essential for blood-brain barrier integrity in central nervous system disease. Nat. Med. 23, 450–460. https://doi.org/10.1038/nm.4309.

41. Dorfel, M.J., and Huber, O. (2012). Modulation of tight junction structure and function by kinases and phosphatases targeting occludin. J. Biomed. Biotechnol. 2012, 807356. https://doi.org/10.1155/2012/807356.

42. Suzuki, T., Elias, B.C., Seth, A., Shen, L., Turner, J.R., Giorgianni, F., Desiderio, D., Guntaka, R., and Rao, R. (2009). PKC eta regulates occludin phosphorylation and epithelial tight junction integrity. Proc. Natl. Acad. Sci. USA 106, 61–66. https://doi.org/10.1073/pnas.0802741106.

43. Yamamoto, M., Ramirez, S.H., Sato, S., Kiyota, T., Cerny, R.L., Kaibuchi, K., Persidsky, Y., and Ikezu, T. (2008). Phosphorylation of claudin-5 and occludin by Rho kinase in brain endothelial cells. Am. J. Pathol. 172, 521–533. https://doi.org/10.2353/ajpath.2008.070076.

44. Elias, B.C., Suzuki, T., Seth, A., Giorgianni, F., Kale, G., Shen, L., Turner, J.R., Naren, A., Desiderio, D.M., and Rao, R. (2009). Phosphorylation of tyr-398 and tyr-402 in occludin prevents its interaction with ZO-1 and destabilizes its assembly at the tight junctions. J. Biol. Chem. 284, 1559–1569. https://doi.org/10.1074/jbc.M804783200.

45. Jin, Z., Tietjen, I., Bu, L., Liu-Yesucevitz, L., Gaur, S.K., Walsh, C.A., and Piao, X. (2007). Disease-associated mutations affect GPR56 protein trafficking and cell surface expression. Hum. Mol. Genet. 16, 1972–1985. https://doi.org/10.1093/hmg/ddm144.

STAR★METHODS

KEY RESOURCES TABLE

REAGENT or RESOURCE	SOURCE	IDENTIFIER
Antibodies		
HA-antibody	Santa Cruz Biotech.	Cat#:7392; RRID:AB_627809
Occludin antibody	Proteintech	Cat#: 13409-1-AP:AB_2156308
Phospho-Occludin (Tyr287) Polyclonal Antibody	ThermoFisher Scientific	Cat#: PA5-105344; RRID:AB_2816772
Phospho-Occludin (Thr382) Polyclonal Antibody	ThermoFisher Scientific	Cat#: PA5-105056; RRID:AB_2816529
Phospho-Occludin (Ser507) Polyclonal Antibody	ThermoFisher Scientific	Cat#: PA5-105057; RRID:AB_2816530
IgG from mouse serum	Millipore Sigma	Cat#: I8765; RRID:AB_1163672
Anti-Mouse IgG (whole molecule)–Peroxidase antibody produced in goat	Millipore Sigma	Cat#: A4416; RRID:AB_258167
Anti-Rabbit IgG (whole molecule)–Peroxidase antibody produced in goat	Millipore Sigma	Cat#: A6154; RRID:AB_258284
Anti-ADGRF1(GPR110) antibody	Millipore Sigma	Cat#: HPA038438; RRID:AB_10672645
Alexa Fluor™ Plus 555, anti-Rabbit	Thermo Fisher Scientific	Cat#: A32732; RRID:AB_2633281
Chemicals, peptides, and recombinant proteins		
HA peptide	Thermo Fisher Scientific	Cat#: 26184
Succinimidyl suberate (DSS)	Thermo Fisher Scientific	Cat#: A39267
Halt™ Protease Inhibitor Cocktail	Thermo Fisher Scientific	Cat#: 78430
Fetal bovine serum	Millipore Sigma	Cat#: F2442
Lipofectamine 2000	Thermo Fisher Scientific	Cat#: 11668-019
Opti-mem Reduced serum medium	Thermo Fisher Scientific	Cat#: 31985-070
SimplyBlue SafeStain	Thermo Fisher Scientific	Cat#: LC6060
Restore™ Western Blot Stripping Buffer	Thermo Fisher Scientific	Cat#: 21059
PBS (pH 7.4, without calcium and magnesium)	Thermo Fisher Scientific	Cat#: 10010-031
Acetonitrile, LC-MS grade	JT. Baker	Cat#: UN1648
Water, LC-MS grade	JT. Baker	Cat#: 9831-03
NuPAGE™ LDS Sample Buffer (4X)	Thermo Fisher Scientific	Cat#: NP0007
TRIzol™ Reagent	Thermo Fisher Scientific	Cat#: 15596026
High-Capacity cDNA Reverse Transcription Kit	Thermo Fisher Scientific	Cat#4368814
Power SYBR™ Green PCR Master Mix	Thermo Fisher Scientific	Cat#: 4368708
TaqMan™ Fast Advanced Master Mix	Thermo Fisher Scientific	Cat#: 4444557
MOPS SDS running buffer	Thermo Fisher Scientific	Cat#: NP0001
Dynabeads™ Protein G	Thermo Fisher Scientific	Cat#: 10004D
Dynabeads™ M-280 Streptavidin	Thermo Fisher Scientific	Cat#: 11205D
Trizma® hydrochloride solution (Tris-HCl, pH 7.4)	Sigma	Cat#: T2194-1L
Formic acid	Thermo Fisher Scientific	Cat#: 28905
Trifluoroacetic acid	Thermo Fisher Scientific	Cat#: 28904
Enhanced chemiluminescent (ECL) substrate	Thermo Fisher Scientific	Cat #: 34080
Sulfo-NHS Biotin	Thermo Fisher Scientific	Cat#: 21217
Glycine hydrochloride	Millipore Sigma	Cat#: G2879
Synaptamide	This paper	N/A
Biotinylated-synaptamide	This paper	N/A
Trypsin/Lys-C mix	Promega	Cat#: V5073
DL-Dithiothreitol	Millipore Sigma	Cat#: D9779
Iodoacetamide	Millipore Sigma	Cat#: I1149

Continued

REAGENT or RESOURCE	SOURCE	IDENTIFIER
Ammonium bicarbonate	Millipore Sigma	Cat#: A6141
Dimethyl sulfoxide	Millipore Sigma	Cat#: D2650-5X10ML
Tween-20	Fisher Scientific	Cat#: BP337-500
Tris buffered saline	Santa Cruz	Cat#: sc-362305
Precision plus protein standards	Bio-Rad	Cat#: 161-0374
Cell lysis buffer	Cell Signaling Tech.	Cat#: 9803
PMSF	Cell Signaling Tech.	Cat#: 8553
BSA	Millipore Sigma	Cat#: 126609
Vitamin E	Millipore Sigma	Cat#: T3251
Dextran	Millipore Sigma	Cat#: 31390
Rhodamine 800	Millipore Sigma	Cat#: 83701
Hanks' balanced salt solution	Thermo Fisher Scientific	Cat#: 14175079
MCDB 131 Medium	Thermo Fisher Scientific	Cat#: 10372019
DPBS	Thermo Fisher Scientific	Cat#: 14190144
Paraformaldehyde	Thermo Fisher Scientific	Cat#: J19943-K2
Goat Serum	Millipore Sigma	Cat#: G9023
DAPI	Millipore Sigma	Cat#: D9542
Eagle's Minimum Essential Medium (EMEM)	ATCC	Cat#: 30-2003
Dulbecco's Modified Eagle's Medium (DMEM)	ATCC	Cat#: 30-2002
Critical commercial assays		
Dual-Glo® Luciferase Assay	Promega	Cat#: E2920
Deposited data		
Mass spectrometry raw data	https://www.ebi.ac.uk/pride/	PXD041011
Experimental models: Cell lines		
HEK293 cells	ATCC	Cat#: CRL-1573
GloResponse™ CRE-luc2P HEK293	Promega	Cat#: E8500
Experimental models: Organisms/strains		
C57BL/6 mice	This paper	N/A
Oligonucleotides		
Primers for Real time PCR see Table S1	This paper	N/A
Software and algorithms		
Mascot Distiller	Matrix Science	N/A
Progenesis QI for Proteomics software	Waters Corporation	N/A
Kodak 1D imaging analysis software	Eastman Kodak Company	N/A
Other		
NuPAGE™ 4 to 12%, Bis-Tris, 1.0–1.5 mm, Mini Protein Gels	ThermoFisher Scientific	Cat#: NP0336BOX
Trans-blot turbo transfer pack	Bio-Rad	Cat#: 1704156
C-18 ZipTip pipette tips	Millipore	Cat#: ZTC18S096
Acclaim PepMap100 C18 trap column	ThermoFisher Scientific	Cat#: 164535
Acclaim RSLC column	ThermoFisher Scientific	Cat#: 164534
stainless steel emitter	Fisher Scientific	Cat#: ES542

RESOURCE AVAILABILITY

Lead contact

Further information and requests for resources and reagents should be directed to and will be fulfilled by the lead contact, Hee-Yong Kim (hykim@nih.gov).

Materials availability

Plasmids generated in this study are available upon request.

Data and code availability

Raw mass spectrometry data have been deposited to the ProteomeXchange Consortium via the PRIDE[1] partner repository with the dataset identifier PXD041011.

This paper does not report original code.

Any additional information required to reanalyze the data reported in this paper is available from the lead contact upon request.

EXPERIMENTAL MODEL AND SUBJECT DETAILS

Mice

C57BL/6 mice were obtained from NIH-NCI animal facility. GPR110 heterozygous mice on C57BL/6 background were generated by Knockout Mouse Project (KOMP) Repository. Heterozygote mating of GPR110 KO mice were conducted in our laboratory. All experiments in this study were carried out in accordance with the guiding principles for the care and use of animals approved by the National Institute on Alcohol Abuse and Alcoholism (LMS-HK13). GPR110 KO and WT adult mice (6 months) were used in the BBB permeability study. P0 pups and adult WT mice (6 months) were used for brain microvessel preparations. Both female and male adult mice were used for these experiments.

Cell culture

HEK293 cells (ATCC, CRL-1573) and GloResponse™ CRE-luc2P HEK293 cells (Promega, E8500) were maintained in EMEM and DMEM, respectively, supplemented with 10% fetal bovine serum (FBS). Cells were cultured at 37°C and 5% CO2.

METHOD DETAILS

Plasmid constructs

C-terminal HA-tagged human GPR110 construct containing full-length open reading frame sequence of human GPR110 (NM_153840.2) (GPR110-HA), F663S mutant, and control empty vector M45 were obtained from GeneCopoeia (Rockville, MD).

Transfection of HEK293 cells

HEK293 cells were seeded at a 15-cm dish overnight and transfected with GPR110-HA or GPR110 F663S or empty vector M45 for 24 h using Lipofectamine 2000 in accordance with manufacturer's instructions. Five μg plasmid DNA, 50 μL Lipofectamine 2000, and 1400 μL of Opti-mem reduced-serum medium were used for transfection.

Chemical crosslinking in living cells

In cell crosslinking was performed as described previously.[21] Transfected HEK293 cells were washed one time with PBS (pH 7.4), resuspended in 5 mL of PBS and incubated with 1 mM DSS for 30 min at room temperature (25°C). The crosslinking reaction was quenched by Tris-HCl (pH 7.4). The cells were lifted and transferred to a 15-mL conical tube. After pelleted by centrifugation at 1000 rpm for 5 min at 4°C, the cells were lysed in 1.5 mL lysis buffer containing protease cocktail and 1mM PMSF on ice for 40 min with brief vortexing every 5 min. Cell debris was removed by centrifugation at 15,000 rcf and the supernatant was collected for immunopurification.

Synaptamide stimulation

After 24 h transfection, the medium was replaced with FBS-free EMEM. After 6 h, cells were incubated with 10 nM synaptamide for desired time points before replacing the medium with PBS for chemical crosslinking.

Purification of GPR110

Cell lysates were incubated with 40 μL of HA antibody overnight before adding 40 μL Dynabeads protein G beads for additional 4 h incubation at 4°C. After washing three times with lysis buffer, the immunoprecipitates were eluted by incubating with 50 μL of 1 mg/mL HA peptide dissolved in the lysis buffer at 30°C for 20 min.

SDS-PAGE, in-gel digestion and desalting

Immunopurified proteins were mixed with 4x lithium dodecyl sulfate (LDS) sample buffer at 30°C for 30 min. Samples were loaded onto 10-well 4-12% Bis-Tris gels. Electrophoresis was carried out at a constant voltage of 200 V using MOPS SDS running buffer for approximate 60 min. Proteins were stained with Coomassie blue in accordance with manufacturer's instruction. Selected protein bands were excised for reduction/alkylation and tryptic digestion as described.[21] The tryptic peptides were dried by vacuum centrifugation and resuspended with 0.1% TFA. After desalting using C-18 ziptip using manufacturer's protocol, the peptide solution is concentrated briefly by vacuum centrifugation to remove acetonitrile prior to nano-HPLC/MS-MS analysis.

Nano-HPLC MS/MS analysis

Nano-LC-ESI-MS/MS was performed on a Thermo Scientific Orbitrap Fusion Lumos Tribrid Mass Spectrometer equipped with an Ultimate 3000 HPLC system. The mobile phases consisted of 0.1% formic acid (solvent A) and 0.1% formic acid in 98% ACN (solvent B). Five μL of peptide samples were loaded onto an Acclaim PepMap100 C18 trap column (Thermo Fisher Scientific). Peptides were separated by a 15-cm Acclaim RSLC column (Thermo Fisher Scientific) at a flow rate of 300 nL/min with a gradient from 4-35% solvent B in 95 min. LC eluent was sprayed into the MS instrument with a stainless steel emitter (Fisher Scientific) using a spray voltage of 2.2 kV in positive-ion mode. Full scan spectra from m/z 350 to 1700 at resolution of 120,000 were acquired in the Orbitrap. Data-dependent MS/MS spectra were acquired in the ion trap using CID with a normalized energy of 30. Dynamic exclusion for the already fragmented precursor ions was used with the following parameters: exclusion duration 30 s, exclude after 1 time, repeat duration 30 s, and mass tolerance 10 ppm. Charge states of 2-6 were included for fragmentation.

Identification of proteins

MS/MS data were searched against the NCBInr human database with Mascot (v2.3.2, Matrix Science) using Mascot Distiller (2.3.2.0) as the data input filter. Search parameters were set as follows: enzyme, trypsin; precursor ion mass tolerance, 10 ppm; fragment ion mass tolerance, 0.3Da; maximum missed cleavages allowed 2; carbamidomethyl of cysteine residues for fixed modification; oxidation of methionine and addition of 156. 07864 Da on lysine or N-terminal (end-capping modification) for variable modification. The criteria used to filter results included 1% false positive threshold and expect value of less than 0.05 for significant peptide matches. The expect score was calculated using the homology threshold or the significance threshold as per a standard Mascot protein family report.

Label-free protein quantitation

Spectra acquired from biological triplicate were loaded (Thermo raw files) into the Progenesis QI for Proteomics software (version 1.05156.29278) for label-free protein quantitation as described previously with minor modification.[21] Automatic alignment of chromatograms and automatic peak-picking settings were used to process the data. Features with charge of 1 and charge > 7 were filtered out for the analysis. Normalization to all proteins was performed based on the assumption that a significant number of features were unaffected across different sample runs. Peptide and protein identifications were performed using Mascot search engine via Mascot Distiller. A Mascot score corresponding to a p-value of 0.05 was set as a threshold for peptide identifications. Proteins were quantitated from non-conflicting features. Results of the peptide and protein measurements were exported as Excel files.

Western blot analysis

Samples were electrophoresed in 4-12% Bis-Tris gels at 200 V using MOPS SDS running buffer. Proteins were transferred to a PVDF membrane (Bio-Rad) at 25 V for 30 min using a Bio-Rad Trans-Blot Turbo transfer system. The membrane was blocked with 5% milk in TBS containing 0.1% Tween 20 (TBS-T) at room temperature for 1 h. Blots were washed three times with TBS-T, incubated with primary antibody (1/1000 dilution ratio, in TBS-T containing 5% BSA and 0.1% sodium azide) at 4°C overnight, washed three times with TBS-T, and incubated with peroxidase-conjugated secondary antibody for 1 h at room temperature. After washing three times with TBS-T, blots were incubated with enhanced chemiluminescent (ECL) substrates for 5 min before imaged with a Kodak Gel Logic 440 Imaging system or Azura Sapphire Biomolecular Imager. Band intensity was quantitated using Kodak 1D imaging analysis software.

Luciferase assay for cAMP activity

Luciferase assay was performed as described previously.[8] GloResponse™ CRE-luc2P HEK293 cells containing a luciferase gene (luc2P) (Promega) were seeded in 24-well plates at 2.5×106 cells/well, transfected with F663S, or WT GPR110-HA, or empty vector M45 for 24 h, and stimulated with 10 nM synaptamide in DMEM containing 0.01% BSA and 40 µM vitamin E. Experiments without transfection were performed in parallel to subtract the background noise. After 16 h, the cells were measured for the CRE activity using the Dual-Glo® Luciferase assay kit (Promega) following the manufacturer's instructions.

Immunocytochemistry

HEK cells were cultured and transfected with F663S or GPR110-HA for 48 h on poly-lysine coated glass cover slips. Cells were washed with PBS, fixed in 2% paraformaldehyde (PFA) 10 min at room temperature, and washed three times with PBS at 4°C. Non-specific binding was blocked with detergent-free blocking buffer containing 10% goat serum and 1% BSA at 4°C. The cells were incubated with anti-GPR110 monoclonal antibody overnight at 4°C, washed three times for 10 min with PBS, and incubated with Alexa 555-conjugated goat anti-rabbit (1:500 dilution, Thermo Fisher Scientific) and DAPI for 1 h at room temperature. After washed three times with PBS a cover slip was attached to the cells with fluoromount. The mounted cells were observed under a LSM700 Confocal microscopy (Zeiss, Germany).

Cell surface biotinylation

HEK293 cells were transfected with F663S, WT GPR110-HA, or empty vector (M45) for 24 h. The cells were washed with ice-cold PBS and incubated with 0.5mg/mL Sulfo-NHS Biotin (Thermo Fisher Scientific) in PBS for 1 h in 4°C.[45] After washing 4 times with PBS containing 100 mM glycine, the cells were lysed with lysis buffer (Cell Signaling Tech) for 30 min on ice. Cell debris was cleared by centrifugation (12,000 rpm) and soluble cell lysate were incubated with 50 µl Dynabeads M-280 streptavidin beads for 1 h at 4°C. Beads were washed three times with lysis buffer and then incubated with 50 µl 2×LDS in 4°C for 30 min. Biotinylated GPR110 were detected by Western blotting using HA-antibody.

Isolation and evaluation of cerebral microvessels

Microvessel isolation from pup (P0) or adult mouse brain cortex was performed according to the protocol described by Lee et al.[31] Three adult mice or 8-9 pups were used for each isolation. The structure of microvessels was evaluated by microscopy. The cellular compositions of the microvessel preparations were evaluated by RT-qPCR of Tjp1 (endothelial marker), Aqp4 (astrocyte end-foot marker) and Anpep (pericyte marker).

Real time quantitative PCR (RT-qPCR)

RNA from microvessels and cortical tissues was extracted with TRIzol™ Reagent (Thermo Fisher Scientific) according to the manufacturer's instructions. One hundred ng of the RNA was used for reverse transcription using High-Capacity cDNA Reverse Transcription Kit (Thermo Fisher Scientific). cDNAs were synthesized in thermal cycler that was set on 25°C for 10 min, 37°C for 120 min, and 85°C for 5 min. The cDNA was mixed with the Power SYBR™ Green PCR Master Mix (Thermo Fisher Scientific) or TaqMan™ Fast Advanced Master Mix (Thermo Fisher Scientific) and targeting oligomers followed by amplification using Quant Studio 3 (Applied biosystem). Hypoxanthine phosphoribosyltransferase (HPRT) and GAPDH were used for normalization of the TagMan and SYBR™ Green assays, respectively. Oligomer and TaqMan probe information are detailed in Table S1.

Evaluation of the BBB permeability using near infrared fluorescence imaging

Near infrared fluorescent tracer injection was performed as described[30,32] with modification. Briefly, 100 µL of Rhodamine 800 (R800, 496 Da) at 1 mg/mL in PBS was injected intravenously into the tail vein in adult mice (6 months, WT or GPR110 KO). After 2 h the anesthetized animals were perfused for 5 min with Hanks' balanced salt solution (HBSS). After perfusion, brains were removed and put on a 2 mm thick slide on ice. The accumulation of R800 dye was examined *ex vivo* using an Azure Sapphire Biomolecular Imager. Images were acquired was at several z-axis levels (ex784nm/λem823nm) and quantified with Kodak 1D imaging analysis software.

QUANTIFICATION AND STATISTICAL ANALYSIS

Significance was determined by Student's t-test using Excel. P values < 0.05 were considered significant. Data are presented as mean $\pm$ SEM (standard error of the mean) of at least three independent experiments.